

Estimating timber volume loss due to storm damage in Carinthia, Austria, using ALS/TLS and spatial regression models

Arne Nothdurft^{*1}, Christoph Gollob¹, Ralf Kraßnitzer¹, Gernot Erber²,
Tim Ritter¹, Karl Stampfer², and Andrew O. Finley³

¹University of Natural Resources and Life Sciences, Vienna (BOKU), Department of Forest and Soil Sciences, Institute of Forest Growth, Austria

²University of Natural Resources and Life Sciences, Vienna (BOKU), Department of Forest and Soil Sciences, Institute of Forest Engineering, Austria

³Department of Forestry, Michigan State University, East Lansing, MI 48824-1222,
USA

June 17, 2021

A spatial regression model framework is presented to predict growing stock volume loss due to storm Adrian which caused heavy forest damage in the upper Gail valley in Carinthia, Austria, in October 2018. Model parameters were estimated using growing stock volume measured with a terrestrial laser scanner on 62 sample plots distributed across five sub-regions. Predictor variables were derived from high resolution vegetation height measurements collected during an airborne laser scanning campaign. Non-spatial and spatial candidate models were proposed and assessed based on fit to observed

^{*}arne.nothdurft@boku.ac.at, Tel: +43-1-47654-91411

data and out-of-sample prediction. Spatial Gaussian processes associated model intercepts and regression coefficients were used to capture spatial dependence. Results show a spatially-varying coefficient model, which allowed the intercept and regression coefficients to vary spatially, yielded the best fit and prediction. Two approaches were considered for prediction over blowdown areas: 1) an *areal* approach that viewed each blowdown as a single prediction unit indexed by its centroid; and 2) a *block* approach where each blowdown was partitioned into smaller prediction units to better align with sample plots' spatial support. Joint prediction was used to acknowledge spatial dependence among block units. Results demonstrated the block approach is preferable as it mitigated change-of-support issues encountered in the areal approach. Despite the small sample size, predictions for 55% of the total 564 blowdown areas, accounting for 93% of the total loss, had a coefficient of variation less than 25%. Key advantages of the proposed regression framework and chosen Bayesian inferential paradigm, were the ability to quantify uncertainty in spatial covariance parameters, propagate parameter uncertainty through to prediction, and provide statistically valid prediction point and interval estimates for individual blowdowns and collections of blowdowns at the sub-region and region scale via posterior predictive distribution summaries.

Keywords: Storm damage, Small area estimation, Bayesian regression model, Space-varying coefficients, Gaussian Process

1 Introduction

Analyses by [Schelhaas et al. \(2003\)](#) showed that storms were responsible for more than half the total damages in European forests for the period 1950–2000. The majority of this forest damage occurred in the Alpine zone of mountainous regions. In Austria, for the period 2002–2010, storms damaged 3.1 million m³ annually ([Thom et al., 2013](#)),

representing 0.26 % of the total growing stock as well as 12 % of the total annual fellings. In Switzerland, the storm damage was 17 and 22 times higher in the period 1985–2007 than in the two preceding 50 years periods (Usbeck et al., 2010).

According to Usbeck et al. (2010), the possible explanations for such an increasing trend were manifold and include increased growing stocks, enlarged forested area, milder winters and hence tendency for wet and unfrozen soils, and higher recorded maximum gust wind speeds. Since 1990, 85 % of all primary damage in the Western, Central and Northern European regions was caused by catastrophic storms with maximum gust wind speed between 50–60 ms⁻¹ (Gregow et al., 2017). The relevance of storm damage is likely to increase, as simulations with climate scenario data and forest stand projections suggested a higher probability of exceeding the critical wind speed and, hence, wind throw events (Olofsson and Blennow, 2008; Blennow et al., 2010). Such a trend could negatively impact the carbon balance, especially in Western and Central European regions (Lindroth et al., 2009).

Wind throw events have direct and indirect impact on long-term sustained yield planning. A common indirect cost stems from the fact that storm-felled trees provided a surplus of breeding material for bark beetles and promoted their rapid population increase causing extra timber losses in the subsequent years (Marini et al., 2016). Hence, it is recommended that fallen trees be removed within two years of the disturbance (Groot et al., 2018). Following a wind throw event and prior to harvesting the storm-felled trees, strategic salvage harvest planning is needed (Jirikowski and Pröll, 2003). Implementing such plans requires unplanned/unbudgeted logging road and site development efforts as well as interaction with external harvesting, transportation, and processing industry.

To inform strategic salvage harvest planning, a rapid and accurate estimate of the spatial extent and local severity of damage is needed. The task is to provide such estimates for individual and collections of discrete blowdowns. In most situations, a paucity of existing field inventory data within or adjacent to blowdowns precludes design-based estimation. Rather, field data from an existing set of sparsely sampled inventory plots or a small purposively selected set of sample plots, can be coupled with auxiliary

data using a model to yield viable estimates. In such settings, the forest response variable measured on sample plots is regressed against meaningful auxiliary data. Commonly, such auxiliary data come as remotely sensed variables collected via satellite, aircraft, or unmanned aerial vehicle (UAV) based sensors. Remotely sensed data are routinely used to support forest inventories and have been shown to increase accuracy and precision of the estimates, and reduce field data collection efforts; see [Köhl et al. \(2006\)](#) and other references herein.

Increasingly, laser imaging detection and ranging (LiDAR) data are being incorporated into forest inventory and mapping efforts. LiDAR measurements offer high-resolution and 3-dimensional (3D) representation of forest canopy structure metrics that are often related to forest variables of interest. For example, LiDAR height metrics have been successfully used to estimate average tree height ([Magnussen and Boudewyn, 1998](#)), stem density ([Næsset and Bjercknes, 2001](#)), basal area ([Næsset, 2002](#); [Magnussen et al., 2010](#)), biomass ([Finley et al., 2017](#); [Babcock et al., 2018](#)) and growing stock volume ([Nelson et al., 1988](#); [Næsset, 1997](#); [Maltamo et al., 2006](#)).

In practice, different techniques are used to predict forest variables using field measurements and remote sensing data. Nonparametric imputation methods, using some flavor of nearest neighbor (NN) interpolation ([Moeur and Stage, 1995](#)), achieved robust prediction for possibly multivariate response variable vectors ([Tomppo and Halme, 2004](#); [LeMay and Temesgen, 2005](#); [Maltamo et al., 2006](#); [Packalén and Maltamo, 2007](#)). [Hudak et al. \(2008\)](#) demonstrated the NN prediction accuracy can be enhanced through resampling and classifications with “random forests” ([Breiman, 2001](#)). A key shortcoming of NN imputation methods, however, is the lack of statistically robust variance estimates, with the exception of some approximations presented and assessed in [McRoberts et al. \(2007, 2011\)](#) and [Magnussen \(2013\)](#).

Similar to NN imputation methods, geostatistical methods yield accurate and precise spatial prediction of forest variables. Additionally, geostatistical methods provide a solid theoretical foundation for probability-based uncertainty quantification, see, e.g., [Ver Hoef and Temesgen \(2013\)](#). In such settings, point-referenced observations are in-

dexed by spatial locations, e.g., latitude and longitude, and predictive models build on classical kriging methods (Cressie, 1993; Schabenberger and Gotway, 2004; Chilès and Delfiner, 2012). Additional flexibility for specifying and estimating regression mean and covariance components comes from recasting these predictive models within a Bayesian inferential framework (Banerjee et al., 2014). Similar extensions and benefits have been demonstrated for data with observations indexed by areal units, particularly in small-area estimation settings, many of which build on the Fay-Harriot model (Fay and Herriot, 1979), see, e.g., Ver Planck et al. (2017); Ver Planck et al. (2018) and references therein.

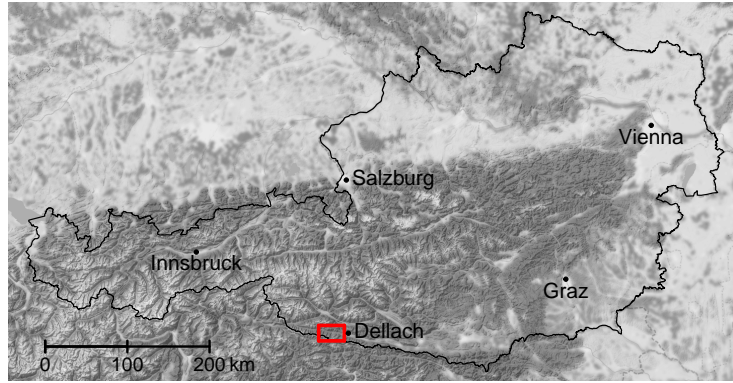
Following the study region description and data in Section 2.1, a general model that subsumes various sub-models is developed in Section 2.2 along with implementation details for parameter estimation, prediction, and model selection in Section 2.3. Here too, we offer two different approaches for prediction over the areal blowdown units. Results presented in Section 3 focus first on model selection then comparison among blowdown predictions, which is followed by discussion in Section 4. Some final remarks and future direction are provided in Section 5.

2 Materials and methods

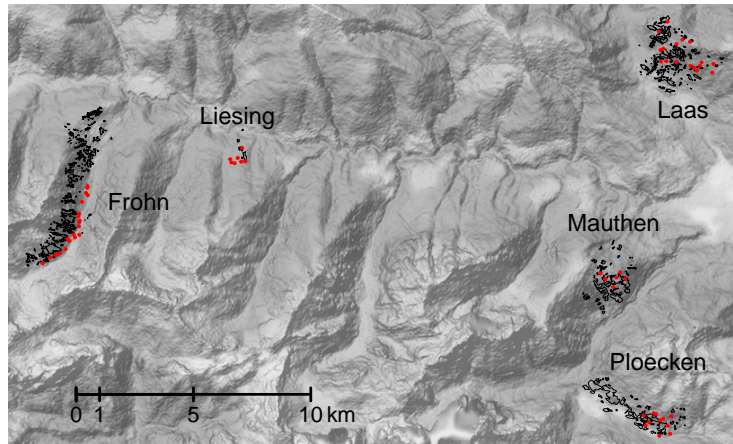
2.1 Study region and model data

The study region was located in the southern region of the Austrian federal state of Carinthia, within the upper Gail valley and near the Dellach forest research and training center, which is jointly operated by the Institute of Forest Growth and the Institute of Forest Engineering of the University of Natural Resources and Life Sciences Vienna (Figure 1(a)). On October 28, 2018, the storm Adrian formed over the western Mediterranean Sea and achieved wind gust speeds of 130 km/h throughout Carinthia. Within 72 hours, the storm was producing 627 l/m² of precipitation at the Plöckenpass meteorological station, located near the study region, and inflicting heavy damage on the region's forest (Zimmermann, 2018).

Forest blowdown, caused by Adrian, was widely distributed across the Hermagor ad-



(a)



(b)

Figure 1: (a) Location of the study region in Southern Carinthia, Austria. (b) Storm damage areas (polygons) and sample plots (red dots) in the study region.

ministrative district (Bezirk), which covers the study region. Using high-resolution aerial images provided by the Carinthian Forest Service, blowdown occurrences in the district were identified and delineated with high accuracy. As illustrated in Figure 1(b) the blowdowns were concentrated in five distinct sub-regions labeled Frohn, Laas, Liesing, Mauthen, and Ploecken. A total of 564 blowdowns were delineated, totalling 212.3 ha of affected forest. Table 1 provides the number of blowdown occurrences across the sub-regions and affected area characteristics.

Table 1: Summary statistics of the digitized blowdowns and collected sample plot data by sub-region.

	Blowdown areas						Sample plots					
	Area (ha)						Growing stock volume (m ³ /ha)					
	n	mean	med	sd	min	max	N	mean	med	sd	min	max
Frohn	273	0.230	0.065	0.600	0.004	7.231	21	593	579	227	188	979
Laas	152	0.362	0.138	0.565	0.004	2.727	17	785	772	333	142	1382
Liesing	5	0.581	0.348	0.621	0.115	1.607	7	689	698	67	563	757
Mauthen	62	0.621	0.190	1.075	0.013	4.969	6	762	748	323	403	1220
Ploecken	72	0.738	0.242	1.724	0.008	12.322	11	773	773	136	528	968
Total	564	0.376	0.110	0.892	0.004	12.322	62	705	730	256	142	1382

Forest inventory data were not available for the study region; therefore, a field measurement campaign was initiated in May 2020 (post-Adrian) to collect growing stock timber volume measurements suitable for estimating volume loss due to blowdown. A total of $n=62$ sample plots were installed in unaffected forest adjacent to blowdowns (Figure 1(b)). Plot locations were chosen to characterize forest similar in structure and composition to the pre-blowdown forest. No plots were located within blowdowns. Plot measurements were conducted using the terrestrial laser scanning (TLS) GeoSLAM ZEB HORIZON system (GeoSLAM Ltd., Nottingham, UK). Position and diameter at breast height (DBH) for the approximately 5586 measurement trees were derived from 3D point clouds on a 20 m radius plot using fully automated routines demonstrated in [Gollob et al. \(2019, 2020\)](#) and in [Ritter et al. \(2017, 2020\)](#). Tree height was estimated using a Näslund function formulated as a mixed-effects model with plot-level random effects. Stem volume was calculated using a traditional stem-form function ([Pollanschütz, 1965](#)). For each plot, growing stock timber volume was expressed as m³/ha (i.e., computed as the sum of tree volume scaled by the 7.958 fixed-area plot tree expansion factor). Table 1 provides a summary of growing stock timber volume by sub-region, the values of which

serve as the response variable observations in subsequent regression models.

The Carinthian Forest Service provided a comprehensive set of aerial laser scanning (ALS) variables summarized on a $1\text{ m} \times 1\text{ m}$ resolution grid collected in 2012 over the study region. Within each grid cell, ALS variables comprised the point cloud height distribution's mean, median, min, maximum, and standard deviation. Values for each variable in this fine grid were averaged over each plot to yield a set of plot-level predictor variables to pair with the growing stock volume response variable.

2.2 Model construction

As stated in Section 1, the study goal was to predict what 2020 growing stock timber volume in blowdowns would have been if not destroyed by Adrian in late October 2018. Sample plot data, which included 2020 response variable measurements and 2012 ALS predictor variables, were used to develop models to predict growing stock timber volume for blowdowns where only 2012 ALS measurements were available.

Due to the relatively small number of sample plots within any one of the five spatially disjoint sub-regions (Figure 1), we aimed to pool the 62 sample plot measurements. An ideal pooled model would allow for intra- and inter-location specific relationships between the response and predictor variables. Such spatially varying relationships are particularly attractive because they accommodate potential impact of unobserved (and for the most part unobservable) spatially-explicit mediating factors such as disturbance history, genetics, and local growth environments. When cast within a regression framework, a spatially varying coefficients (SVC) model uses a smoothly-varying spatial process to pool information and avoid overfitting (Gelfand et al., 2003; Finley, 2011).

Given prediction is our primary goal, a preferred model would also estimate residual spatial correlation (i.e., spatial dependence among measurements not explained by the predictor variables) and use it to improve prediction performance. We anticipated the residual spatial correlation would decrease as distance between measurements increased. Again, following Gelfand et al. (2003) and broader geostatistical literature cited in Section 1, residual spatial dependence is effectively estimated using a spatial process.

To accommodate the anticipated data features, assess varying levels of model complexity, and deliver statistically valid probabilistic uncertainty quantification we model response $y(\mathbf{s})$ at generic spatial location \mathbf{s} as

$$y(\mathbf{s}) = (\beta_0 + \delta_0 w_0(\mathbf{s})) + \sum_{j=1}^p x_j(\mathbf{s}) \{\beta_j + \delta_j w_j(\mathbf{s})\} + \epsilon(\mathbf{s}), \quad (1)$$

where $x_j(\mathbf{s})$, for each $j = 1, \dots, p$, is the known value of a predictor variable at location \mathbf{s} , β_j is the regression coefficient corresponding to $x_j(\mathbf{s})$, β_0 is an intercept, and $\epsilon(\mathbf{s})$ follows a normal distribution with mean zero and variance τ^2 . Here, τ^2 is viewed as the measurement error variance. The quantities $w_0(\mathbf{s})$ and $w_j(\mathbf{s})$ are spatial random effects corresponding to the intercept and predictor variables, respectively, thereby yielding a spatially varying regression model. To allow for varying levels of model complexity, the δ s in Equation (1) are binary indicator variables used to turn on and off the spatial random effects (i.e., a value of 1 means the given spatial random effect is included in the model and 0 otherwise). When $\delta = 1$ the associated space-varying regression coefficient can be seen as having a global effect, i.e., β_0 or β_j s, with local adjustments, i.e., $w_0(\mathbf{s})$ or $w_j(\mathbf{s})$ s.

Over n locations, a given spatial random effect $\mathbf{w} = (w(\mathbf{s}_1), w(\mathbf{s}_2), w(\mathbf{s}_3), \dots, w(\mathbf{s}_n))^\top$ follows a multivariate normal distribution with a length n zero mean vector and $n \times n$ covariance matrix Σ with $(i, j)^{th}$ element given by $C(\mathbf{s}_i, \mathbf{s}_j; \boldsymbol{\theta})$. Clearly, for any two generic locations \mathbf{s} and \mathbf{s}^* locations within the study region the function used for $C(\mathbf{s}, \mathbf{s}^*; \boldsymbol{\theta})$ must result in a symmetric and positive definite matrix Σ . Such functions are known as positive definite functions, details of which can be found in [Cressie \(1993\)](#), [Chilès and Delfiner \(2012\)](#), and [Banerjee et al. \(2014\)](#), among others. Here we specify $C(\mathbf{s}, \mathbf{s}^*; \boldsymbol{\theta}) = \sigma^2 \rho(\mathbf{s}, \mathbf{s}^*; \boldsymbol{\phi})$ where $\boldsymbol{\theta} = \{\sigma^2, \boldsymbol{\phi}\}$ and $\rho(\cdot; \boldsymbol{\phi})$ is a positive support correlation function with $\boldsymbol{\phi}$ comprising one or more parameters that control the rate of correlation decay and smoothness of the process. The spatial process variance is given by σ^2 , i.e., $\text{Var}(w(\mathbf{s})) = \sigma^2$. This covariance function yields a *stationary* and *isotropic* process, i.e., a process with a constant variance and a correlation depending only on the Euclidean distance separating locations. The Matérn correlation function is a flexible

class of correlation functions with desirable theoretical properties (Stein, 1999) and is given by

$$\rho(\|\mathbf{s} - \mathbf{s}^*\|; \boldsymbol{\phi}) = \frac{1}{2^{\nu-1}\Gamma(\nu)}(\phi\|\mathbf{s} - \mathbf{s}^*\|)^{\nu}\mathcal{K}_{\nu}(\|\mathbf{s} - \mathbf{s}^*\|; \phi); \phi > 0, \nu > 0, \quad (2)$$

where $\|\mathbf{s} - \mathbf{s}^*\|$ is the Euclidean distance between \mathbf{s} and \mathbf{s}^* , $\boldsymbol{\phi} = \{\phi, \nu\}$ with ϕ controlling the rate of correlation decay and ν controlling the process smoothness, Γ is the Gamma function, and \mathcal{K}_{ν} is a modified Bessel function of the third kind with order ν . While it is theoretically ideal to estimate both ϕ and ν , it is often useful from a computational standpoint to fix ν and estimate only ϕ . For our current analysis, such a concession is reasonable given there is likely little information gain in estimating both parameters. Conveniently, when $\nu = 0.5$ the Matérn correlation reduces to the exponential correlation function, i.e., $\rho(\|\mathbf{s} - \mathbf{s}^*\|; \phi) = \exp(-\phi\|\mathbf{s} - \mathbf{s}^*\|)$. Therefore, only two process parameters are estimated for any given random effect are $\boldsymbol{\theta} = \{\sigma^2, \phi\}$.

In the subsequent analysis, we consider the following candidate models defined using the general model (1):

1. Non-spatial—all δ are set to zero. This is simply a multiple regression model.
2. Space-varying intercept (SVI)— δ_0 equals 1 and all other δ s are set to zero. This model estimates a spatial process and associated parameters $\boldsymbol{\theta}_0$ for the intercept, but the impact of the covariates is assumed to be the same across the study region.
3. Space-varying coefficients (SVC)—all δ s are set to 1. This model allows all regression coefficients to vary spatially over the study region. Each spatial process has its own parameters $\boldsymbol{\theta}_0$ and $\boldsymbol{\theta}_j$ for $j = (1, 2, \dots, p)$.

2.3 Implementation and analysis

To facilitate uncertainty quantification for model parameters and subsequent prediction, the Non-spatial, SVI, and SVC candidate models defined in Section 2.2 were fit within a Bayesian inferential framework, see, e.g., Gelman et al. (2013) for a general description Bayesian model fitting methods. The candidate models' Bayesian specification is

completed by assigning prior distributions to all parameters. Then, parameter inference follows from posterior distributions that are sampled using Markov chain Monte Carlo (MCMC) algorithms. [Finley and Banerjee \(2020b\)](#) provide open source software, available in R ([R Core Team, 2020](#)), that implement efficient MCMC sampling algorithms for Equation (1) and associated sub-models. More specifically, the `spSVC` function within the `spBayes` package ([Finley and Banerjee, 2020a](#)) provides MCMC-based parameter posterior summaries, fit diagnostics for model comparison, and prediction at unobserved locations.

Data and annotated R code needed to fully reproduce the analysis and results will be provided as Supplementary Material upon publication or if requested by reviewers.

2.3.1 Prediction

Our interest is in predicting the 2020 growing stock timber volume response variable $\tilde{\mathbf{y}} = (\tilde{y}(\mathbf{s}_1), \tilde{y}(\mathbf{s}_2), \dots, \tilde{y}(\mathbf{s}_{n_0}))^\top$ at a set of n_0 locations where it is not observed but ALS predictors are available (we used tilde to indicate a prediction). Following [Gelman et al. \(2013\)](#) and [Banerjee et al. \(2014\)](#), given MCMC samples from the posterior distributions of the posited model’s parameters, composition sampling is used to sample one-for-one from $\tilde{\mathbf{y}}$ ’s posterior predictive distribution (PPD). For example, the Non-spatial model’s l -th PPD sample $\tilde{\mathbf{y}}^{(l)}$ is drawn from the multivariate Normal distribution $MVN\left(\beta_0^{(l)} + \mathbf{X}\boldsymbol{\beta}^{(l)}, \tau^{2(l)}\mathbf{I}\right)$, where $\beta_0^{(l)}$, $\boldsymbol{\beta}^{(l)} = \left(\beta_1^{(l)}, \beta_2^{(l)}, \dots, \beta_p^{(l)}\right)^\top$, and $\tau^{2(l)}$ are the l -th joint samples from the parameters’ posterior distribution, \mathbf{X} is the $n_0 \times p$ matrix of predictors at the n_0 prediction locations, and \mathbf{I} is the $n_0 \times n_0$ identity matrix. The multivariate Normal PPDs for the SVI and SVC models are given in [Finley and Banerjee \(2020b,a\)](#). Importantly, the SVI and SVC candidate models use joint composition sampling to acknowledge the spatial correlation among prediction locations. A given candidate model’s PPD is evaluated using each of its parameter’s M posterior samples, i.e., $l = 1, 2, \dots, M$, to generate M PPD samples for each of the n_0 prediction locations. These PPD samples are summarized analogously to the parameters’ posterior samples. Prediction point estimates could include the PPD mean or median, and interval esti-

mates can be built off the PPD standard deviation or directly expressed using a set of lower and upper percentiles in the form of a credible interval. For example, a point and dispersion estimate for the growing stock timber volume at a prediction location could be the mean and standard deviation over that location’s M PPD samples.

2.3.2 Model selection

Our analysis had two separate model selection steps. First, in an effort to build parsimonious models and reduce possible issues arising from collinearity among the often highly correlated ALS predictor variables, we identified a common set of predictors to use in the three candidate models. Given our focus on prediction, predictor variable selection aimed to minimize prediction error using leave-one-out (LOO) cross-validation among the 62 sample plot measurements. Second, given the common set of predictors, model fit and prediction performance were used to select the “best” candidate model for subsequent blowdown area prediction. Here, again, candidate model prediction performance was assessed using LOO cross-validation among the 62 sample plot measurements.

For the first model selection step, the Non-spatial model was used to select the set of ALS predictor variables that minimized LOO mean squared prediction error (MSPE). As described in Section 2.1, candidate variables were summaries of the ALS point cloud height distribution and included its mean, median, minimum, maximum, and standard deviation. A backward variable selection algorithm, implemented using the `leaps` (Lumley, 2020) and `caret` (Kuhn, 2020) R packages, identified the predictor set that minimized LOO MSPE.

The second model selection step used model fit and LOO prediction measures to identify the “best” model for subsequent blowdown area prediction. The deviance information criterion (DIC) (Spiegelhalter et al., 2002) and widely applicable information criterion (WAIC) (Watanabe, 2010) model fit criterion were computed for each candidate model. DIC equals $-2(L - p_D)$ where L is goodness of fit and p_D is a model penalty term viewed as the effective number of parameters. Two WAIC criteria were computed based on the log pointwise predictive density (LPPD) with $WAIC_1 = -2(LLPD - p_1)$ and

$WAIC_2 = -2(LLPD - p_2)$ where penalty terms p_1 and p_2 are defined by [Gelman et al. \(2014\)](#) just prior to, and in, Equation (1). Models with lower values of DIC, $WAIC_1$, and $WAIC_2$ have better fit to the observed data and should yield better out-of-sample prediction, see [Gelman et al. \(2014\)](#), [Vehtari et al. \(2017\)](#), or [Green et al. \(2020\)](#) for more details on these model fit criteria.

The three candidate models were also assessed based on LOO cross-validation prediction MSPE and continuous rank probability score (CRPS) ([Gneiting and Raftery, 2007](#)). Because MSPE measures only predictive accuracy, CRPS is a preferable measure of predictive skill because it favors models with both high accuracy and precision. Models with lower MSPE and CRPS should yield better blowdown area predictions. In addition to MSPE and CRPS, we computed the percent of holdout observations covered by their corresponding PPD 95% credible interval. Models with an empirical coverage percent close to the chosen PPD credible interval percent are favored.

2.3.3 Blowdown prediction

Given the sample plot dataset and posited model identified using methods in Section 2.3.2, two approaches were used to predict growing stock timber volume for blowdown areas. We refer to the approaches as *areal* and *block* prediction.

The *areal* approach views each blowdown as a single prediction unit indexed by its polygon centroid and predictor variables computed as an average of the $1\text{ m} \times 1\text{ m}$ resolution ALS values over its extent. Figure 2(a) illustrates the mean canopy height ALS variable summarized for blowdowns within a small portion of the Laas sub-region. [Ver Planck et al. \(2018\)](#) had a somewhat similar setting; however, their dataset and inferential goals differed from ours in a few key ways. First, because their sample data came from variable radius plots, it was not possible to spatially align ALS predictors with response variable measurements at the plot-level. As a result, they made the simplifying assumption that, when pooled, response variable measurements were representative of the stand areal unit within which they were observed. This assumption allowed them to spatially align the response and ALS predictor variables at the stand-level. Second, all

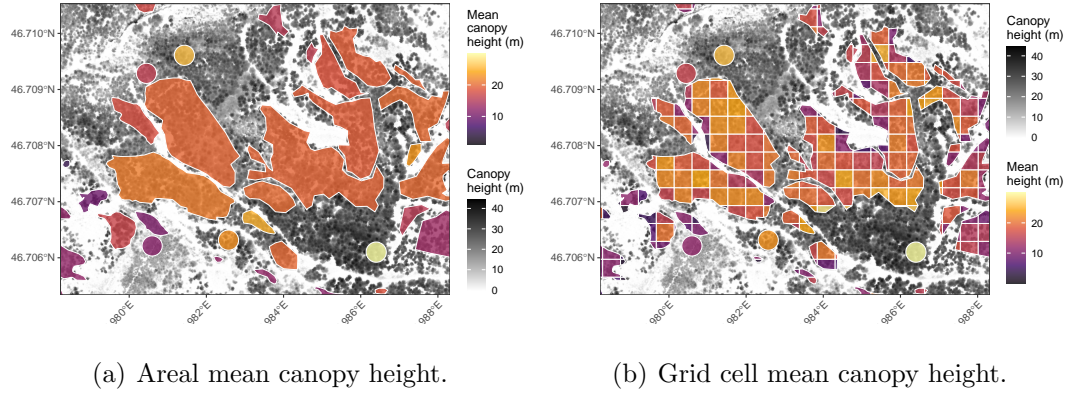


Figure 2: Illustration of the mean canopy height ALS predictor variable used for areal (a) and (b) block prediction for a subset of blowdowns in a small section of the Laas sub-region. The polygons are blowdowns and circles are forest sample plots. The gray scale basemap depicts the $1\text{ m} \times 1\text{ m}$ ALS canopy height grid used to compute the mean canopy height values over plots and blowdown prediction units.

stands within the population held at least two plots and the study goal was to improve stand-level point and interval estimates through a smoothing conditional autoregressive model (CAR) model. In our current setting, the sample data comprise response variable measurements collected on fixed-area plots with clearly defined spatial support over which the ALS predictor variables were also computed—the response and predictor variable measurements are spatially aligned at the plot-level. Also, no sample plots fall within the blowdown prediction units; hence, our inferential goal is squarely on out-of-sample prediction. Despite these differences we pursue the *areal* prediction and clearly acknowledge the change-of-support issue between the discrete fixed-area plot data used to fit the model and different spatial support of the prediction units (see, e.g., [Schabenberger and Gotway \(2004\)](#) for a thorough description of spatial change-of-support problems). While not appropriate from a statistical standpoint, we do see this approach used in practice and therefore include it here for comparison with the *block* approach that mitigates change-of-support issues by better aligning the spatial support of the measurement and prediction units.

For the areal approach, the l -th PPD sample of total growing stock volume (m^3) for a given blowdown is $\tilde{y}_{\mathcal{A}}^{(l)} = A\tilde{y}(\mathbf{s})^{(l)}$, where A is the blowdown’s area (ha) and $\tilde{y}(\mathbf{s})^{(l)}$ is the growing stock volume (m^3/ha) predicted at the blowdown’s centroid \mathbf{s} .

The *block* approach partitions each blowdown into grid cells with the same area as the fixed-area sample plots (i.e., 0.126 ha). Each cell is indexed using its centroid, and predictor variables are computed as an average of the 1 m \times 1 m resolution ALS values over its extent; see illustration in Figure 2(b). Akin to block kriging (Wackernagel, 2003), the response variable prediction for a given blowdown is an aggregate of multiple point predictions within the blowdown extent. More specifically, given a blowdown divided into n_0 cells and corresponding vector holding the l -th joint PPD sample $\tilde{\mathbf{y}}^{(l)}$ (m^3/ha), the PPD sample of total growing stock volume (m^3) for the blowdown is $\tilde{y}_{\mathcal{B}}^{(l)} = \sum_{i=1}^{n_0} a(\mathbf{s}_i)\tilde{y}(\mathbf{s}_i)^{(l)}$, where $a(\mathbf{s}_i)$ is the area of the i -th cell that falls within the blowdown (a_i is at most 0.126 ha when the cell’s extent is completely within the blowdown).

Composition sampling was again used to generate M samples from $\tilde{y}_{\mathcal{A}}$ ’s and $\tilde{y}_{\mathcal{B}}$ ’s PPD for each blowdown. These PPD samples were summarized analogously to the parameters’ posterior samples to yield prediction point, dispersion, and interval estimates for the 564 blowdowns. In addition to blowdown specific PPD summaries, extra composition sampling was used to estimate the total volume PPD by sub-region and region.

3 Results

3.1 Candidate models

Following Section 2.3.2, the model that yielded minimum LOO cross-validation MSPE included only the ALS point cloud height distribution mean predictor variable. We refer to this predictor variable as *mean canopy height* and set it as x_1 in Equation (1) for all candidate models.

Parameter estimates for candidate models are given in Table 2. As expected, the β_1 estimates indicate a strong positive relationship between 2012 mean canopy height and 2020 growing stock volume. The addition of spatial random effects decreased the

Table 2: Parameter posterior distribution median and 95% credible interval for candidate models.

	Non-spatial	SVI	SVC
β_0	159.8 (59.6, 264.1)	172.9 (70.4, 277.5)	176.3 (69.3, 277.8)
β_1	33.7 (27.9, 39.8)	33.2 (27.2, 39)	33 (2.2, 63.9)
σ_0^2		14677.8 (5491.3, 25740.3)	9139.5 (3044.4, 18879.9)
σ_1^2			275.1 (102.1, 1164.2)
ϕ_0		11.6 (1.9, 29.2)	18.7 (4.2, 29.4)
ϕ_1			0.1 (0.03, 3.4)
τ^2	22806.6 (16330.1, 32899.5)	7105.5 (1999, 18985.2)	5721.6 (1927.2, 15421.3)

non-spatial residual variance τ^2 . The reapportionment of τ^2 to σ_0^2 and non-negligible σ_1^2 suggests a substantial portion of variance—not explained by the ALS predictor—had a spatial structure and the ALS predictor had space-varying impact.

The SVI model spatial decay parameter estimates suggest a fairly localized spatial structure. Given the exponential spatial correlation function and km map projection units, the distance d_0 at which the spatial correlation drops to 0.05 (an arbitrary, but commonly used, cutoff) is estimated by solving $0.05 = \exp(-\phi d_0)$ for d_0 providing $d_0 = -\log(0.05)/\phi$. The distance d_0 is commonly referred to as the effective spatial range. Using the SVI model ϕ_0 estimates, the corresponding spatial range is 0.26 (0.10, 1.58) km.

Compared with the SVI model, the SVC model further reduced the non-spatial residual variance by taking into account the space-varying impact of x_1 . Relative to the effective spatial range of the intercept process, the process on x_1 had a long spatial range, i.e., 29.96 (0.88, 99.86) km. That is, the spatially varying slope coefficient for x_1 represented sub-region differences in the relationship between growing stock volume

and mean canopy height that were probably caused by unmeasured species, genetic, or environmental factors.

Table 3: Candidate model fit and leave-one-out (LOO) cross-validation prediction diagnostics. The last three rows were calculated using prediction LOO on the observed data. The row labeled CI Cover is the percent of 95% posterior predictive distribution credible intervals that cover the observed LOO value. Where appropriate, the “best” metric in the row is bolded.

Model	Non-spatial	SVI	SVC
DIC	801.1	752.8	748.7
p_D	3.1	30.4	33.3
L	-397.5	-346.0	-341.0
WAIC ₁	800.7	746.2	738.3
WAIC ₂	801.1	763.8	756.9
p_1	2.8	23.8	22.9
p_2	2.9	32.6	32.2
LPPD	-397.6	-349.3	-346.2
MSPE	23378.4	23134.4	21491.6
CRPS	88.2	87.0	82.9
CI cover	98.4	96.8	98.4

Candidate model fit and LOO cross-validation prediction diagnostics are given in Table 3. Following from Section 2.3.2, the lower values of DIC, WAIC₁, and WAIC₂ indicate addition of spatial random effects to the model intercept and regression slope coefficient improved fit to observed data. Similarly, LOO cross-validation MSPE and CRPS favored the SVC model over the Non-spatial and SVI model. All models achieve an approximate 95% credible interval coverage.

3.2 Blowdown prediction

The SVC model provided the “best” fit and LOO predictive performance (Table 3) and therefore served as the prediction model for the blowdowns. Following methods in Section 2.3.3, areal and block growing stock volume PPD mean and standard deviation were computed for each blowdown, the results of which are plotted in Figure 3. Figure 3(a) shows negligible difference between areal and block PPD means. However, as shown in Figure 3(b), compared with the block approach, the areal prediction resulted in a consistently larger PPD standard deviation. Additionally, supplemental Figure S1 shows the areal PPD coefficient of variation (CV) is generally larger than the block PPD CV.

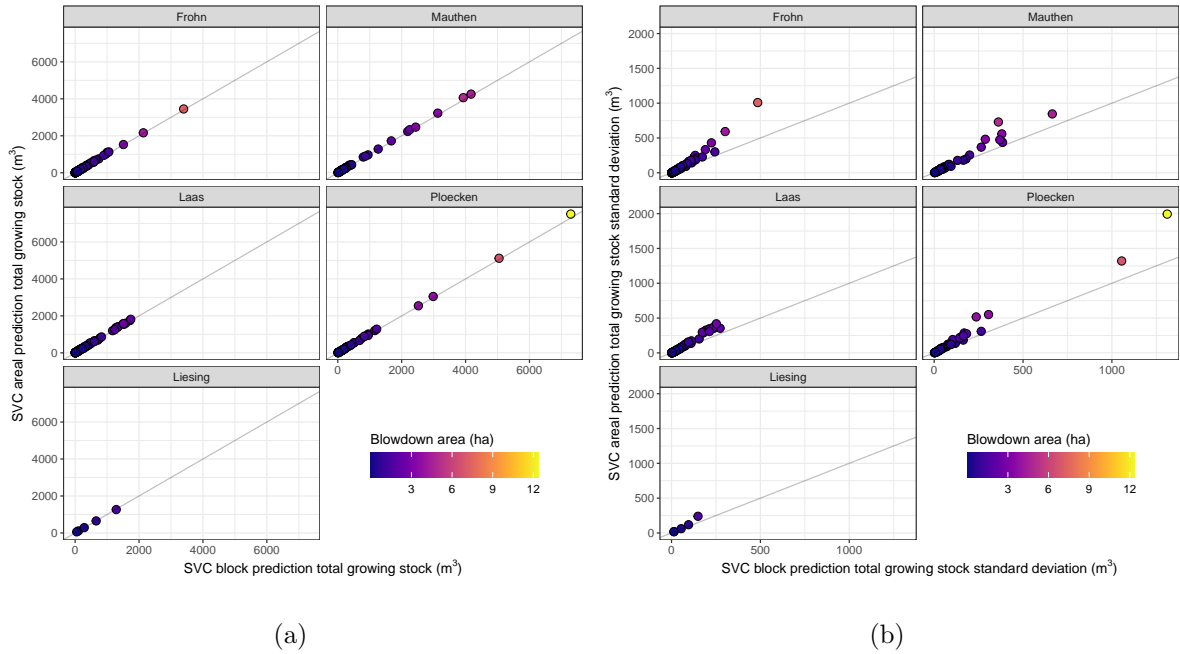


Figure 3: Summaries of each blowdown’s total growing stock volume (m^3) posterior predictive distribution computed using areal and block prediction approach. Points represent blowdowns, colored by area, and broken down by sub-region with a one-to-one line.

Table 4 provides sub-region growing stock volume loss totals and corresponding 95% confidence intervals. Although total blowdown area in Frohn was larger than other sub-regions, its per unit area growing stock loss $510.68 m^3/ha$ ($32,086.1 m^3/62.83 ha$) was

less than that in Laas (637.26 m³/ha), Liesing (818.21 m³/ha), Mauthen (784.76 m³/ha), and Ploecken (638.50 m³/ha). This disparity between Frohn and the other sub-regions is because the blowdowns in the Frohn sub-region were concentrated in relatively unproductive forests close to the alpine treeline zone.

Table 4: *Growing stock volume loss by sub-region and study region posterior predictive distribution median and 95% credible interval.*

	Area (ha)	Volume (m ³)
Frohn	62.83	32086 (28290, 35921)
Laas	54.95	35017 (31293, 38930)
Liesing	2.90	2373 (1941, 2849)
Mauthen	38.49	30205 (25676, 34758)
Ploecken	53.15	33936 (28998, 39361)
Total	212.32	133775 (122935, 144308)

Maps of PPD summaries per blowdown were prepared for each sub-region. For example, Figure 4 shows blowdowns in the Frohn sub-region colored by growing stock volume PPD estimate mean, standard deviation, and coefficient of variation. Similar maps for the other sub-regions are provided in the Supplemental Material.

Figure 5 shows the distribution of PPD CV by blowdown area. The average predicted growing stock volume CV over all blowdowns was 24.6 %, with individual CV predictions ranging from 9.2 % to 70.3 %. Approximately 90 % of blowdown predictions had CVs lower than 33.9 %. Relatively large prediction errors (i.e., large CVs) occurred for the smaller blowdown areas. Blowdowns for which the CV was less than 20 % accounted for 73.2 % of the total damage in the study region, and areas with a CV less than 25 % represented 93.2 % of the total damage.

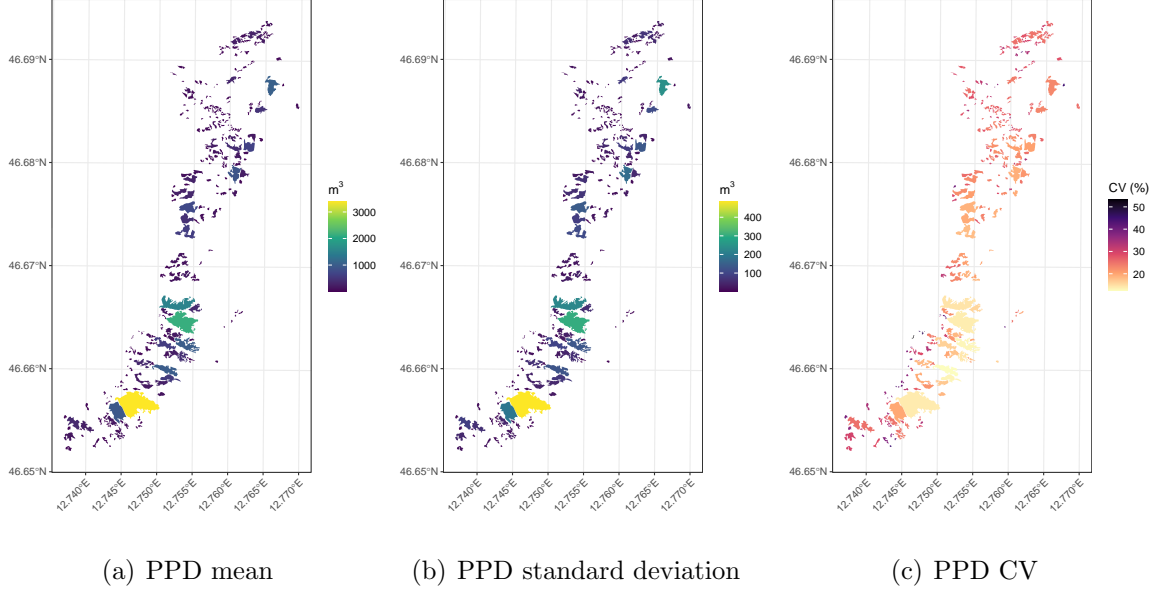


Figure 4: SVC block prediction approach posterior predictive distribution (PPD) mean, standard deviation, and coefficient of variation (CV) of total growing stock volume (m^3) for blowdowns in Frohn sub-region.

4 Discussion

Among the set of ALS predictors, mean canopy height alone explained a substantial portion of the response variable's variance and yielded the lowest LOO cross-validation MSPE. This finding is similar to those in other related studies. For example, [Breidenbach and Astrup \(2012\)](#) selected mean canopy height to predict above-ground biomass using Norwegian national forest inventory data, and [Magnussen et al. \(2014\)](#) selected mean canopy height to predict growing stock density in a study that considered Swiss and Norwegian national forest inventory data. Further, [Mauro et al. \(2016\)](#) identified maximum vegetation height as the only significant predictor in small area estimation models used to improve quadratic mean diameter estimates in Central Spain.

Given the mean canopy height predictor, the SVC model showed consistently better fit and predictive performance compared to the Non-spatial and SVI models (Table 3), and was therefore selected as the model to generate areal and block prediction for the

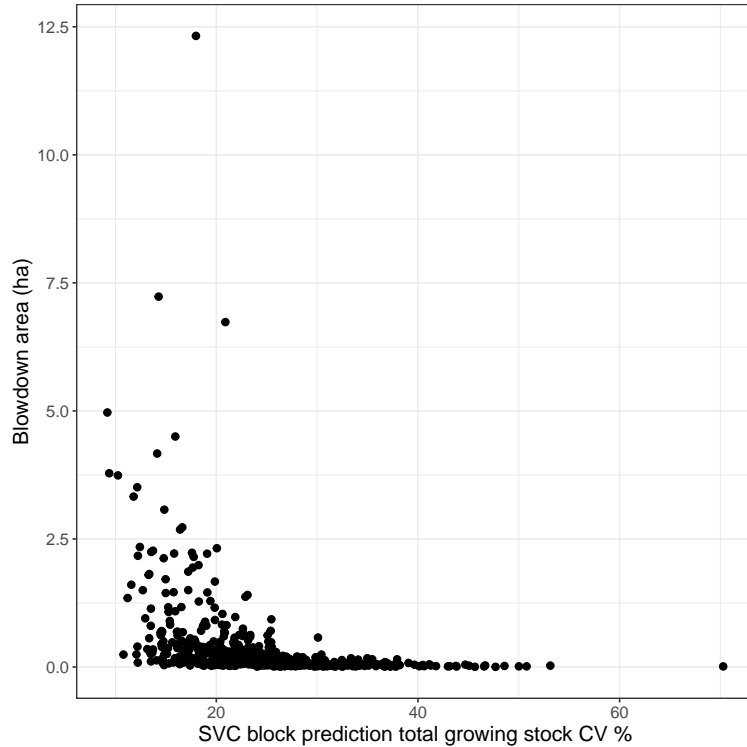


Figure 5: SVC block prediction approach coefficient of variation (CV) posterior predictive distribution versus blowdowns area.

blowdowns.

In regression, and most other modeling contexts, it is assumed the predictor variables used to estimate model parameters are the same as those used in subsequent prediction. This assumption does not hold for the areal prediction approach described in Section 2.3.3, because the ALS variables computed over the 62 0.126 ha sample plots could have a different distribution than the ALS variables computed over the variable area blowdowns. Although it is reasonable to expect the mean of a given ALS variable to be similar between the sample plot and blowdown distributions, the dispersion of the two distributions could be quite different. That is, a change-of-support was immanent between the sample plots (model data) and the prediction units' areal extent. This fact alone should precluded areal prediction application; however, our analysis results further underscore the approach's shortcomings.

In the areal approach each blowdown was considered as a single prediction point, and its predicted volume per unit area was scaled by the blowdown’s area to arrive at the blowdown’s total volume. Such an approach might seem intuitive, but is problematic in the current setting. The issue is akin to how variance scales with forest inventory plot size. It is often the case that a forest variable’s variance is inversely related to the area over which the variable is measured (Freese, 1962). Consequently, a timber volume variable shows more variability when measured on smaller plots than on larger plots, especially when applied to structurally complex forests. This is because the larger plots average over local scale structural variability. When using a single prediction at the blowdown’s centroid, the areal prediction variance does not scale with blowdown area. In contrast, the block approach more accurately scales prediction variance with blowdown area as reflected in Figure 3(b). This is because its PPD is the result of an average over possibly multiple spatially correlated prediction units (grid cells) within the blowdown’s boundary—the number of prediction units contributing to this average scales with blowdown area.

Finally, the PPDs rely on the spatial correlation between observed and prediction locations, e.g., using Equation 2, to appropriately weight the contribution of observed data for prediction. For the areal approach, this correlation is computed between observed locations and a blowdown’s polygon centroid, which is the average location relative to the polygon’s vertices. If the polygon’s shape is highly irregular, with a large boundary length to area ratio, then its centroid might not represent well the distance between observed locations and the polygon’s extent. As an extreme example, the centroid of a polygon in the shape of a letter “C” or “L” will fall outside the polygon boundary. Again, such issues are circumvented using the block prediction approach.

A particularly useful quality of the Bayesian inferential paradigm is PPDs can be generated for any arbitrary set of prediction units from a single grid cell to sets of blowdowns that comprise a sub-region or entire study region. Inference proceeds from desired joint PPD samples. These PPD samples can be summarized using measures of central tendency, dispersion, intervals, and transformations, with results presented as

maps or tables, e.g., Figure 4 and Table 4.

5 Conclusions

The study goal to estimate growing stock timber volume loss due to storm Adrian in the Austrian upper Gail valley in Carinthia, was met using ALS and TLS measurements coupled through a flexible spatial regression model cast within a Bayesian inferential framework. Limited data availability and its configuration in space and time presented several inferential constraints on how statistically robust estimates could be pursued. Our proposed regression model was designed to leverage information from a small set of plot samples and aerial ALS as well as spatial autocorrelation among forest measurements and nonstationary relationships between response and predictor variables.

Three candidate models of varying complexity were assessed using model fit and out-of-sample prediction. Performance metrics supported the SVC model which was then used to make areal and block predictions over the blowdowns. Our results showed that in contrast to the areal approach, the block approach mitigates issues with change-of-support by matching the prediction unit to the sample plot extent. Using this finer spatial scale prediction unit and a joint prediction algorithm that acknowledges spatial correlation among prediction units, the total growing stock volume PPD captures the correlation among prediction units within a given blowdown and scale appropriately with blowdown area. The block prediction approach facilitated statistically sound inference at various spatial scales, i.e., blowdown, sub-region, and region levels.

The proposed methodology and annotated code that yields fully reproducible results can be adapted to deliver damage assessment for other forest disturbance events in future periods and different geographic regions. While additional sample plot data would improve estimates in our current study, we were able to demonstrate a fairly high level of accuracy and precision is achievable using a limited sample size. This small sample, i.e., $n=62$ plots, was collected using a TLS which, compared with traditional individual tree measurements, allowed for time and effort efficient data collection. Based on our

experience from this and other efforts, a field crew can collect ~ 20 -25 plots per day, even in difficult alpine terrain.

Our study illustrated a methodology to efficiently deliver information required for strategic salvage harvesting following storm and other disturbances. Future work focuses on augmenting the SVC model to incorporate large spatial datasets using Nearest Neighbor Gaussian Processes (Finley et al., 2019), automate remote sensing predictor variable selection (Franco-Villoria et al., 2019), and accommodate high-dimensional (Finley et al., 2017; Taylor-Rodriguez et al., 2019) and distributional regression (Umlauf and Kneib, 2018; Stasinopoulos et al., 2018) response vectors to predict forest disturbance induced change in species composition and diameter/size distributions.

6 Acknowledgments

This study was supported by the project Digi4+ and was financed by the Austrian Federal Ministry of Agriculture, Regions and Tourism under project number 101470. Finley was supported by the United States National Science Foundation DMS-1916395 and by NASA Carbon Monitoring System grants. The authors appreciate the support during the fieldwork that was given by the forest owners, Clemens Wassermann, Günter Kronawetter and the team of the Carinthian Forest Service.

References

- Babcock, C., A. O. Finley, H.-E. Andersen, R. Pattison, B. D. Cook, D. C. Morton, M. Alonzo, R. Nelson, T. Gregoire, L. Ene, T. Gobakken, and E. Næsset (2018). Geostatistical estimation of forest biomass in interior alaska combining landsat-derived tree cover, sampled airborne lidar and field observations. *Remote Sensing of Environment* 212, 212–230. 4
- Banerjee, S., B. Carlin, and A. Gelfand (2014). *Hierarchical Modeling and Analysis for*

- Spatial Data, Second Edition*. Chapman & Hall/CRC Monographs on Statistics & Applied Probability. Taylor & Francis. [5](#), [9](#), [11](#)
- Blennow, K., M. Andersson, J. Bergh, O. Sallnäs, and E. Olofsson (2010, 03). Potential climate change impacts on the probability of wind damage in a south swedish forest. *Climatic Change* *99*, 261–278. [3](#)
- Breidenbach, J. and R. Astrup (2012, July). Small area estimation of forest attributes in the norwegian national forest inventory. *European Journal of Forest Research* *131*(4), 1255–1267. [20](#)
- Breiman, L. (2001). Random forests. *Machine Learning* *45*(1), 5–32. [4](#)
- Chilès, J. and P. Delfiner (2012). *Geostatistics: Modeling Spatial Uncertainty*. Wiley Series in Probability and Statistics. Wiley. [5](#), [9](#)
- Cressie, N. A. C. (1993, January). *Statistics for spatial data*. Wiley. [5](#), [9](#)
- Fay, R. E. and R. A. Herriot (1979). Estimates of income for small places: An application of james-stein procedures to census data. *Journal of the American Statistical Association* *74*(366), 269–277. [5](#)
- Finley, A. and S. Banerjee (2020a). *spBayes: Univariate and Multivariate Spatial-Temporal Modeling*. R package version 0.4-3. [11](#)
- Finley, A. O. (2011). Comparing spatially-varying coefficients models for analysis of ecological data with non-stationary and anisotropic residual dependence. *Methods in Ecology and Evolution* *2*(2), 143–154. [8](#)
- Finley, A. O. and S. Banerjee (2020b). Bayesian spatially varying coefficient models in the spbayes r package. *Environmental Modelling & Software* *125*, 104608. [11](#)
- Finley, A. O., S. Banerjee, Y. Zhou, B. D. Cook, and C. Babcock (2017). Joint hierarchical models for sparsely sampled high-dimensional lidar and forest variables. *Remote Sensing of Environment* *190*, 149–161. [4](#), [24](#)

- Finley, A. O., A. Datta, B. D. Cook, D. C. Morton, H. E. Andersen, and S. Banerjee (2019). Efficient Algorithms for Bayesian Nearest Neighbor Gaussian Processes. *Journal of Computational and Graphical Statistics* 28, 401–414. [24](#)
- Franco-Villoria, M., M. Ventrucchi, and H. Rue (2019). A unified view on Bayesian varying coefficient models. *Electronic Journal of Statistics* 13(2), 5334 – 5359. [24](#)
- Freese, F. (1962). *Elementary Forest Sampling*. Agriculture handbook. U.S. Department of Agriculture, Forest Service. [22](#)
- Gelfand, A., H.-J. Kim, S. C.F, and S. Banerjee (2003, 02). Spatial modeling with spatially varying coefficient processes. *Journal of the American Statistical Association* 98, 387–396. [8](#)
- Gelman, A., J. Carlin, H. Stern, D. Dunson, A. Vehtari, and D. Rubin (2013). *Bayesian Data Analysis, Third Edition*. Chapman & Hall/CRC Texts in Statistical Science. Taylor & Francis. [10](#), [11](#)
- Gelman, A., J. Hwang, and A. Vehtari (2014, Nov). Understanding predictive information criteria for bayesian models. *Statistics and Computing* 24(6), 997–1016. [13](#)
- Gneiting, T. and A. E. Raftery (2007). Strictly proper scoring rules, prediction, and estimation. *Journal of the American Statistical Association* 102(477), 359–378. [13](#)
- Gollob, C., T. Ritter, and A. Nothdurft (2020). Forest inventory with long range and high-speed personal laser scanning (pls) and simultaneous localization and mapping (slam) technology. *Remote Sensing* 12(9). [7](#)
- Gollob, C., T. Ritter, C. Wassermann, and A. Nothdurft (2019). Influence of scanner position and plot size on the accuracy of tree detection and diameter estimation using terrestrial laser scanning on forest inventory plots. *Remote Sensing* 11(13). [7](#)
- Green, E., A. Finley, and W. Strawderman (2020). *Introduction to Bayesian Methods in Ecology and Natural Resources*. Springer International Publishing. [13](#)

- Gregow, H., A. Laaksonen, and M. E. Alper (2017, April). Increasing large scale wind-storm damage in western, central and northern european forests, 1951–2010. *Scientific Reports* 7(1), 46397. [3](#)
- Groot, M., N. Ogris, and A. Kobler (2018). The effects of a large-scale ice storm event on the drivers of bark beetle outbreaks and associated management practices. *Forest Ecology and Management* 408, 195–201. [3](#)
- Hudak, A. T., N. L. Crookston, J. S. Evans, D. E. Hall, and M. J. Falkowski (2008). Nearest neighbor imputation of species-level, plot-scale forest structure attributes from lidar data. *Remote Sensing of Environment* 112(5), 2232–2245. Earth Observations for Terrestrial Biodiversity and Ecosystems Special Issue. [4](#)
- Jirikowski, W. and W. Pröll (2003). Krisenmanagement nach Windwurf — Crisis management after windthrow disasters. BFW-Praxisinformation 1/2003: 3-5. [3](#)
- Köhl, M., S. Magnussen, and M. Marchetti (2006). *Sampling Methods, Remote Sensing and GIS Multiresource Forest Inventory*. Springer Berlin Heidelberg. [4](#)
- Kuhn, M. (2020). *caret: Classification and Regression Training*. R package version 6.0-86. [12](#)
- LeMay, V. and H. Temesgen (2005, 04). Comparison of Nearest Neighbor Methods for Estimating Basal Area and Stems per Hectare Using Aerial Auxiliary Variables. *Forest Science* 51(2), 109–119. [4](#)
- Lindroth, A., F. Lagergren, A. Grelle, L. Klemedtsson, O. Langvall, P. Weslien, and J. Tuulik (2009). Storms can cause europe-wide reduction in forest carbon sink. *Global Change Biology* 15(2), 346–355. [3](#)
- Lumley, T. (2020). *leaps: Regression Subset Selection*. R package version 3.1, based on Fortran code by Alan Miller. [12](#)
- Magnussen, S. (2013). An assessment of three variance estimators for the k-nearest neighbour technique. *Silva Fennica* 47(1), 925. [4](#)

- Magnussen, S. and P. Boudewyn (1998). Derivations of stand heights from airborne laser scanner data with canopy-based quantile estimators. *Canadian Journal of Forest Research* 28(7), 1016–1031. [4](#)
- Magnussen, S., D. Mandallaz, J. Breidenbach, A. Lanz, and C. Ginzler (2014). National forest inventories in the service of small area estimation of stem volume. *Canadian Journal of Forest Research* 44(9), 1079–1090. [20](#)
- Magnussen, S., E. Næsset, and T. Gobakken (2010). Reliability of lidar derived predictors of forest inventory attributes: A case study with norway spruce. *Remote Sensing of Environment* 114(4), 700–712. [4](#)
- Maltamo, M., K. Eerikäinen, P. Packalén, and J. Hyypä (2006, 02). Estimation of stem volume using laser scanning-based canopy height metrics. *Forestry: An International Journal of Forest Research* 79(2), 217–229. [4](#)
- Maltamo, M., J. Malinen, P. Packalén, A. Suvanto, and J. Kangas (2006). Nonparametric estimation of stem volume using airborne laser scanning, aerial photography, and stand-register data. *Canadian Journal of Forest Research* 36(2), 426–436. [4](#)
- Marini, L., B. Økland, A. Jönsson, B. Bentz, A. Carroll, B. Forster, J.-C. Grégoire, R. Hurling, L.-M. Nageleisen, S. Netherer, H. Ravn, A. Weed, and M. Schroeder (2016, 11). Climate drivers of bark beetle outbreak dynamics in norway spruce forests. *Ecography*. [3](#)
- Mauro, F., I. Molina, A. García-Abril, R. Valbuena, and E. Ayuga-Téllez (2016). Remote sensing estimates and measures of uncertainty for forest variables at different aggregation levels. *Environmetrics* 27(4), 225–238. [20](#)
- McRoberts, R. E., S. Magnussen, E. O. Tomppo, and G. Chirici (2011). Parametric, bootstrap, and jackknife variance estimators for the k-nearest neighbors technique with illustrations using forest inventory and satellite image data. *Remote Sensing of Environment* 115(12), 3165–3174. [4](#)

- McRoberts, R. E., E. O. Tomppo, A. O. Finley, and J. Heikkinen (2007). Estimating areal means and variances of forest attributes using the k-nearest neighbors technique and satellite imagery. *Remote Sensing of Environment* 111(4), 466–480. 4
- Moeur, M. and A. R. Stage (1995, 05). Most Similar Neighbor: An Improved Sampling Inference Procedure for Natural Resource Planning. *Forest Science* 41(2), 337–359. 4
- Næsset, E. (1997). Estimating timber volume of forest stands using airborne laser scanner data. *Remote Sensing of Environment* 61(2), 246–253. 4
- Næsset, E. (2002). Predicting forest stand characteristics with airborne scanning laser using a practical two-stage procedure and field data. *Remote Sensing of Environment* 80(1), 88–99. 4
- Næsset, E. and K.-O. Bjerknes (2001). Estimating tree heights and number of stems in young forest stands using airborne laser scanner data. *Remote Sensing of Environment* 78(3), 328–340. 4
- Nelson, R., W. Krabill, and J. Tonelli (1988). Estimating forest biomass and volume using airborne laser data. *Remote Sensing of Environment* 24(2), 247–267. 4
- Olofsson, E. and K. Blennow (2008). The probability of wind damage in forestry under a changed wind climate. *Climatic Change* 87(3), 347–360. 3
- Packalén, P. and M. Maltamo (2007). The k-msn method for the prediction of species-specific stand attributes using airborne laser scanning and aerial photographs. *Remote Sensing of Environment* 109(3), 328–341. 4
- Pollanschütz, J. (1965). Eine neue Methode der Formzahl- und Massenbestimmung stehender Stämme - Neue Form- bzw. Kubierungsfunktionen und ihre Anwendung - A new method for the estimation of stem forms. Technical Report 68, Forstliche Bundesversuchsanstalt Mariabrunn. 7
- R Core Team (2020). *R: A Language and Environment for Statistical Computing*. Vienna, Austria: R Foundation for Statistical Computing. 11

- Ritter, T., C. Gollob, and A. Nothdurft (2020). Towards an optimization of sample plot size and scanner position layout for terrestrial laser scanning in multi-scan mode. *Forests* 11(10). [7](#)
- Ritter, T., M. Schwarz, A. Tockner, F. Leisch, and A. Nothdurft (2017). Automatic mapping of forest stands based on three-dimensional point clouds derived from terrestrial laser-scanning. *Forests* 8(8). [7](#)
- Schabenberger, O. and C. Gotway (2004). *Statistical Methods for Spatial Data Analysis*. Chapman & Hall/CRC Texts in Statistical Science. Taylor & Francis. [5](#), [14](#)
- Schelhaas, M.-J., G.-J. Nabuurs, and A. Schuck (2003). Natural disturbances in the european forests in the 19th and 20th centuries. *Global Change Biology* 9(11), 1620–1633. [2](#)
- Spiegelhalter, D. J., N. G. Best, B. P. Carlin, and A. Van Der Linde (2002). Bayesian measures of model complexity and fit. *Journal of the Royal Statistical Society Series B* 64(4), 583–639. [12](#)
- Stasinopoulos, M. D., R. A. Rigby, and F. D. Bastiani (2018). Gamlss: A distributional regression approach. *Statistical Modelling* 18(3-4), 248–273. [24](#)
- Stein, M. (1999). *Interpolation of Spatial Data: Some Theory for Kriging*. Springer Series in Statistics. Springer New York. [10](#)
- Taylor-Rodriguez, D., A. O. Finley, A. Datta, C. Babcock, H.-E. Andersen, B. D. Cook, D. C. Morton, and S. Banerjee (2019). Spatial factor models for high-dimensional and large spatial data: An application in forest variable mapping. *Statistica Sinica* 29, 1155–1180. [33311955\[pmid\]](#). [24](#)
- Thom, D., R. Seidl, G. Steyrer, H. Krehan, and H. Formayer (2013). Slow and fast drivers of the natural disturbance regime in central european forest ecosystems. *Forest Ecology and Management* 307, 293–302. [2](#)

- Tomppo, E. and M. Halme (2004). Using coarse scale forest variables as ancillary information and weighting of variables in k-nn estimation: a genetic algorithm approach. *Remote Sensing of Environment* 92(1), 1–20. 4
- Umlauf, N. and T. Kneib (2018). A primer on bayesian distributional regression. *Statistical Modelling* 18(3-4), 219–247. 24
- Usbeck, T., T. Wohlgemuth, M. Dobbertin, C. Pfister, A. Bürgi, and M. Rebetez (2010). Increasing storm damage to forests in switzerland from 1858 to 2007. *Agricultural and Forest Meteorology* 150(1), 47–55. 3
- Vehtari, A., A. Gelman, and J. Gabry (2017, Sep). Practical bayesian model evaluation using leave-one-out cross-validation and waic. *Statistics and Computing* 27(5), 1413–1432. 13
- Ver Hoef, J. M. and H. Temesgen (2013, 03). A comparison of the spatial linear model to nearest neighbor (k-nn) methods for forestry applications. *PLOS ONE* 8, 1–13. 4
- Ver Planck, N. R., A. O. Finley, and E. S. Huff (2017). Hierarchical bayesian models for small area estimation of county-level private forest landowner population. *Canadian Journal of Forest Research* 47(12), 1577–1589. 5
- Ver Planck, N. R., A. O. Finley, J. A. Kershaw, A. R. Weiskittel, and M. C. Kress (2018). Hierarchical bayesian models for small area estimation of forest variables using lidar. *Remote Sensing of Environment* 204, 287–295. 5, 13
- Wackernagel, H. (2003). *Multivariate Geostatistics: An Introduction with Applications*. Springer Berlin Heidelberg. 15
- Watanabe, S. (2010). Asymptotic equivalence of bayes cross validation and widely applicable information criterion in singular learning theory. *J. Mach. Learn. Res.* 11, 3571–3594. 12
- Zimmermann, N. (2018). Tief VAIA sorgt für Regen über 400 mm, Hochwasser und Sturm. UBIMET GmbH, Vienna. <https://uwz.at/de/a/>

tief-vaia-sorgt-fuer-regen-ueber-400-mm-hochwasser-und-foehn-sturm.

Accessed: 2021-04-09. 5

Supplemental material

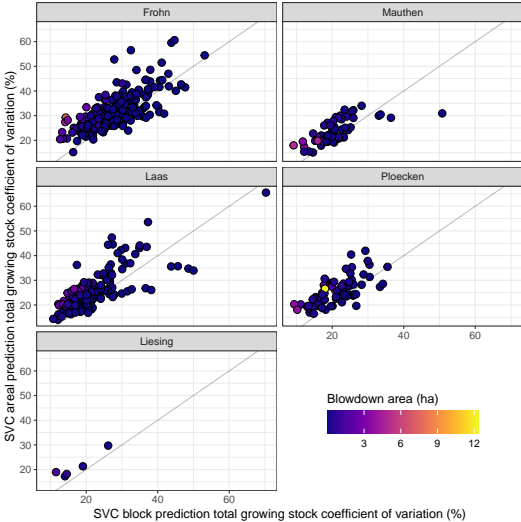
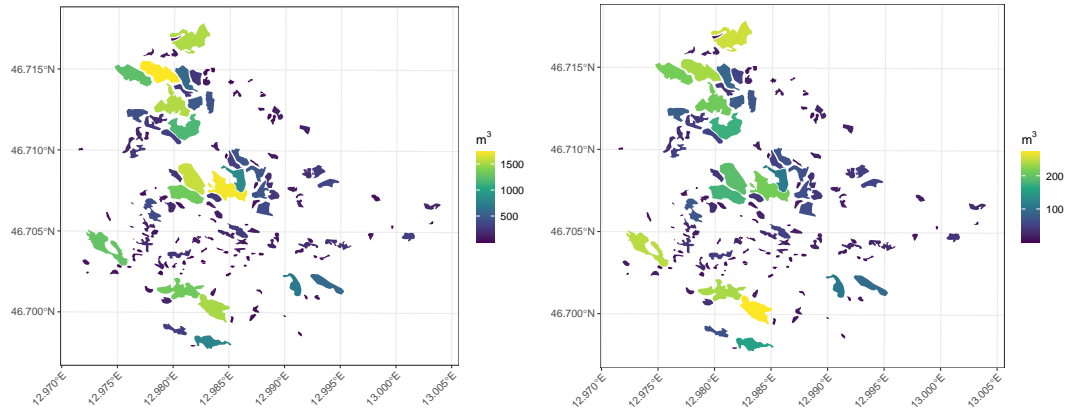
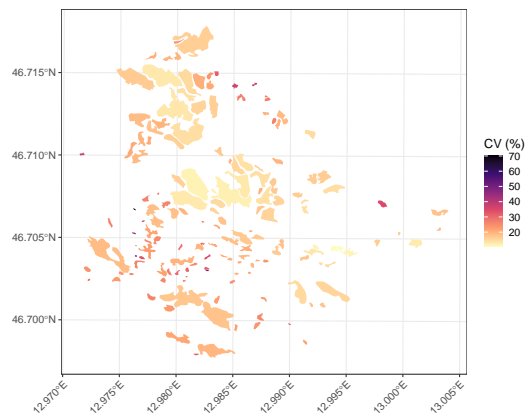


Figure S1: Summaries of each blowdown's total growing stock volume (m^3) posterior predictive distribution computed using areal and block prediction approach. Points represent blowdowns, colored by area, and broken down by sub-region with a one-to-one line.



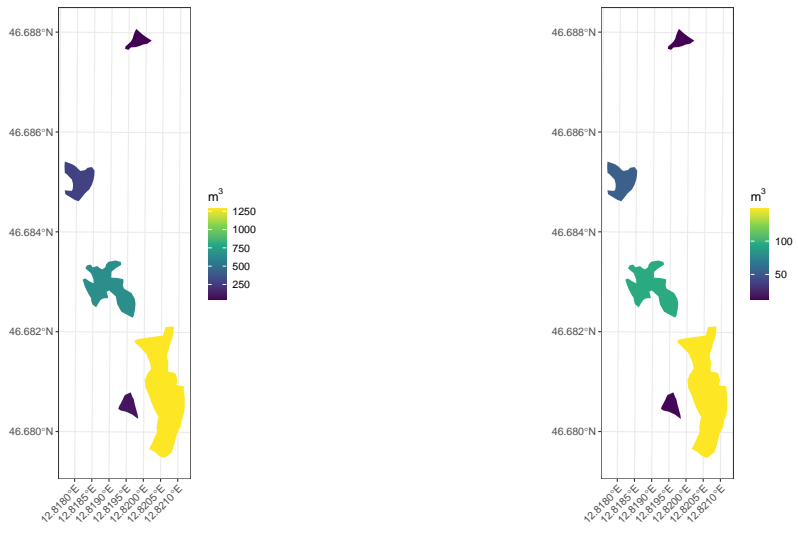
(a) Posterior mean

(b) Posterior standard deviation



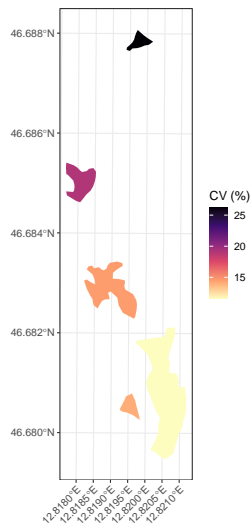
(c) Posterior coefficient of variation

Figure S2: Posterior predictive distribution summaries for the blowdowns in Laas sub-region.



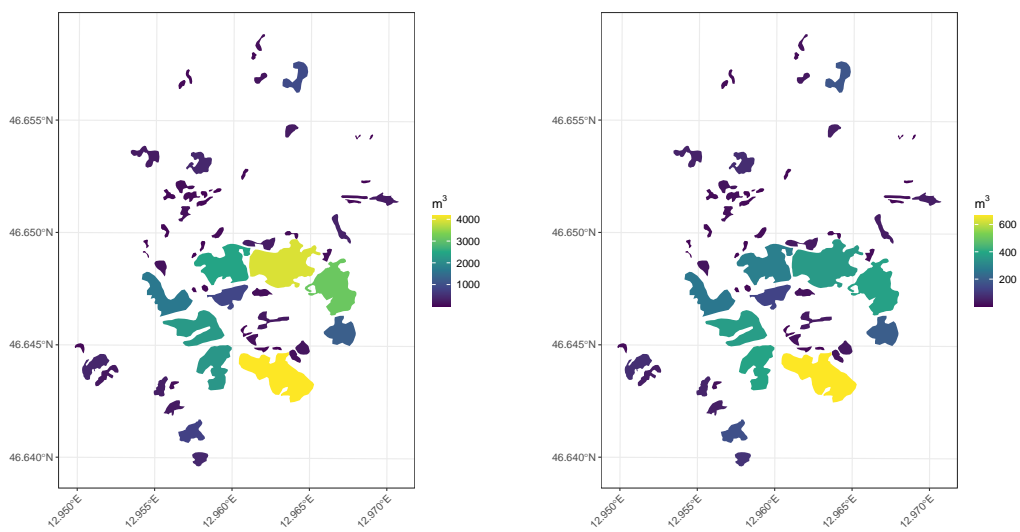
(a) Posterior mean

(b) Posterior standard deviation



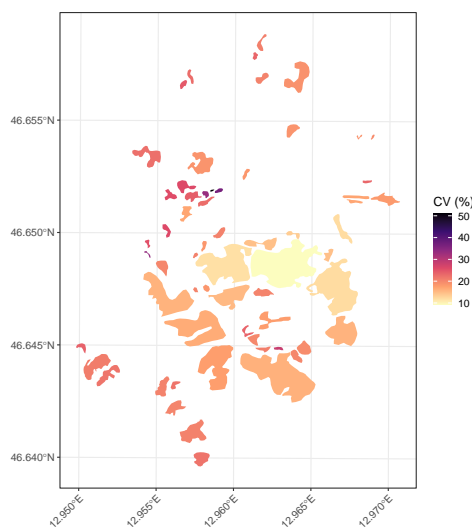
(c) Posterior coefficient of variation

Figure S3: Posterior predictive distribution summaries for the blowdowns in Liesing sub-region.



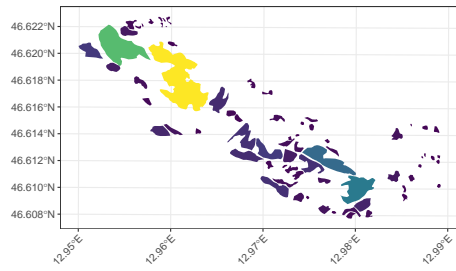
(a) Posterior mean

(b) Posterior standard deviation

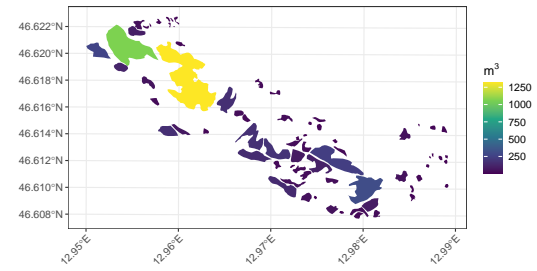


(c) Posterior coefficient of variation

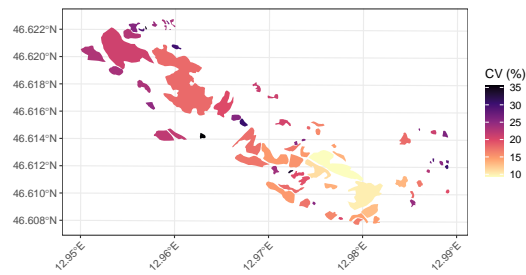
Figure S4: Posterior predictive distribution summaries for the blowdowns in Mauthen sub-region.



(a) Posterior mean



(b) Posterior standard deviation



(c) Posterior coefficient of variation

Figure S5: Posterior predictive distribution summaries for the blowdowns in Plöcken sub-region.